Transfer of Biologically Derived Nanometer-Scale Patterns to Smooth Substrates

Kenneth Douglas, Genevieve Devaud, Noel A. Clark

Atomic force microscopy has been used to measure the surface profile of a periodic array of 10-nanometer (nm)-diameter holes fabricated by fast-atom beam milling of a smooth graphite surface in which a 3.5-nm-thick titanium oxide screen was used as a mask. The nanostructured titanium oxide mask was itself derived from a protein crystal template. Pattern transfer from the biological crystal to the metal oxide film and finally to the graphite substrate was accomplished entirely by parallel processing.

We report the use of atomic force microscopy (AFM) to probe the topography of a periodically nanostructured surface. In these experiments, two-dimensional (2-D) protein crystals are adsorbed to smooth substrates and overcoated with a 1.2-nm Ti thin film that subsequently oxidizes in air to TiO_x. Fast-atom beam (FAB) milling of this composite structure causes the protein crystal to act as a template for patterning the TiO_x film into a screen having a periodic array of nanometer dimension holes with the periodicity of the underlying lattice (22 nm) (*1*). Here we demonstrate that this metal oxide screen can act as a mask for the pattern transfer of a periodic array of holes to the underlying carbon surface. This method provides an inexpensive, "benchtop," intrinsically parallel technique for the periodic nanostructuring of surfaces. Among the applications of this process would be the creation of 2-D ordered sites for subsequent etching to form periodic nanostructures with novel electronic or optical properties (such as periodic luminescent silicon) or to increase the effective surface area, thereby enhancing adhesion or surface activity.

The 2-D crystalline protein monolayers that are used as templates form the surface layer (S-layer) of the bacterial species, *Sulfolobus acidocaldarius*. S-layers are isolated by a modification of the procedure outlined by Michel and Neugebauer (*2*). These protein templates (~1 μm in diameter) were deposited onto smooth substrates and evaporatively coated with metal at 50° from normal incidence with ~1.2 nm of Ti, as measured by a crystal monitor in vacuo. The Ti thin film subsequently oxidizes in air and has been measured by AFM and spectroscopic ellipsometry to be 3.5 nm thick. The overall composition by spectroscopic ellipsometry was found to be $TiO_{1.9}$. These films are then FAB-milled at normal incidence (Fig. 1).

Images obtained by transmission electron microscopy (TEM) and AFM (Fig. 2) show a portion of a metallized S-layer characterized by hexagonal symmetry with a 22-nm periodicity (on–S-layer). Adjacent to the S-layer is an area where the Ti is deposited directly on the carbon substrate (off–S-layer). The TEM and AFM provide different but complementary information about the structure of the metallized S-layer before and after milling. Contrast in TEM is due to mass thickness variation, with the lightest areas being the thickest, whereas the AFM images surface topography, with the lightest areas being the highest.

The images before FAB milling in Fig. 2, A (TEM) and C (AFM), show that the TiO_x thin film is flat and of uniform thickness off–S-layer and exhibits a periodic thickness variation and surface-height modulation on–S-layer. The AFM surface profile plot of Fig. 3A, taken on the line indicated in Fig. 2C, measures the on–S-layer modulation amplitude as ~3 nm and the peak on–S-layer height as ~6 nm above the TiO_x surface. These values reflect an S-layer thickness which is less than that reported from freeze-dried samples; this difference may be attributable to shrinkage caused by air-drying of the S-layer sheets (*3*). The after-milling images (Fig. 2, B and D) show that the TiO_x thin film on–S-layer is modified by the FAB milling and forms a mesh composed of a periodic array of 10-nm holes. Off–S-layer, random holes appear on the substrate, likely the result of localized contamination on the otherwise smooth surfaces. The postmilling TEM image shows that the remaining metal oxide mesh is continuous and that the TiO_x is almost completely removed from all of the holes. The lightest areas shown by TEM in Fig. 2B represent areas of greatest mass thickness around the circumference of the holes, indicating material in excess of the planar TiO_x film (gray background). The holes appear black where the carbon substrate is exposed. Continued milling eventually causes complete loss of the metal oxide overlayer, as manifested by gradual islanding and final disappearance. The after-milling AFM image shows that the holes penetrate both the TiO_x film and the graphite substrate, both on– and off–S-layer. The AFM profile of Fig. 3B, taken on the line in Fig. 2D, shows that after FAB milling the protein layer is collapsed somewhat, possibly by shallow implantation of the Ar atoms; the peak on–S-layer height is now ~4 nm above the TiO_x surface. The off–S-layer holes are as deep as 4.5 nm below the graphite surface. The on–S-layer holes, as measured from the graphite surface, are etched ~1.5 nm into the graphite. The difference between the on–S-layer and off–S-layer hole depths, ~3 nm, may be attributed to the additional height of the protein structures that protrude into the pores on–S-layer (*4*). This "hole punching" is not observed in milled, bare highly oriented pyrolytic graphite, although slight (~2 Å root-mean-square) surface roughening is found, similar to that observed by Eklund *et al.* (*5*).

Insight into the hole formation process can be obtained by quantitative analysis of hole profiles. The structure of individual holes is more easily measured off–S-layer because each hole is isolated from the others. Hole profiles were directly measured by AFM. The inset of Fig. 4 shows a scale profile of a 7.5-nm-deep hole. Volumes were calculated by numerical integration

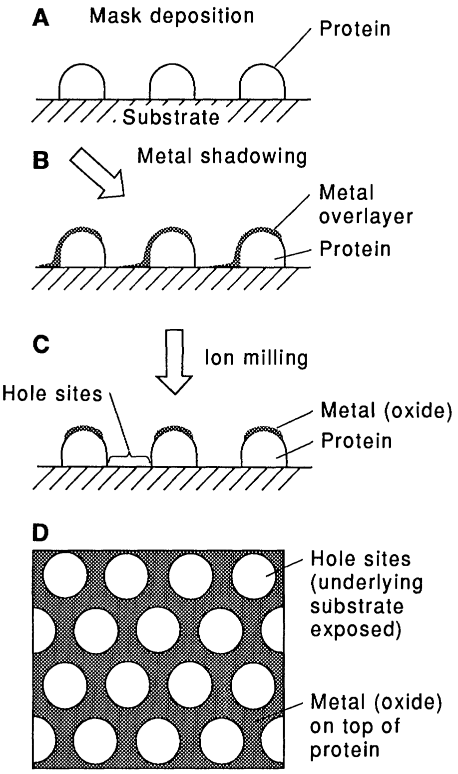

Fig. 1. Processing steps to fabricate nanostructures by templating operation. (**A**) Deposition of protein crystals onto substrate. (**B**) Shadow metallization of protein by electron beam evaporation of Ti (1.2 nm). (**C**) FAB milling to remove metal from substrate, leaving TiO_x-coated protein. (**D**) Plan view of idealized nanostructure.

Department of Physics, University of Colorado, Boulder, CO 80309.

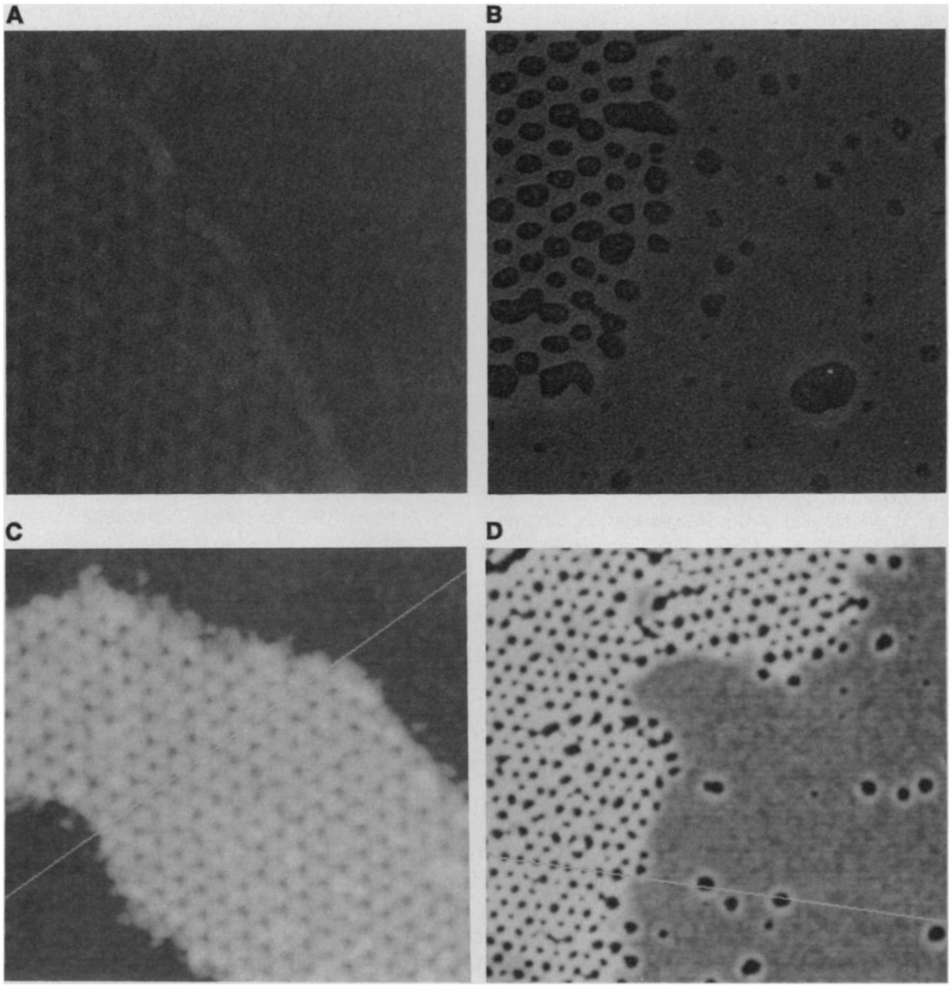

Fig. 2. Images of TiO_x-coated on–S-layer and off–S-layer areas before and after FAB milling. All of the images show both the 2-D hexagonal lattice on–S-layer as well as smooth off–S-layer areas. The lattice parameter of 22 nm serves to indicate the scale length for each image. The substrates used for TEM imaging were electron-beam–deposited amorphous carbon films that were 20 nm thick. For AFM, freshly cleaved highly oriented pyrolytic graphite was used, providing an atomically smooth surface. The AFM images were obtained with a Digital Instruments Nanoscope II AFM in air at room temperature. The TEM was done with a JEOL 100C. (**A**) Before-milling TEM. (**B**) After-milling TEM. (**C**) Before-milling AFM. (**D**) After-milling AFM. Cross-section profiles along the lines in the AFMimages are shown in Fig. 3.

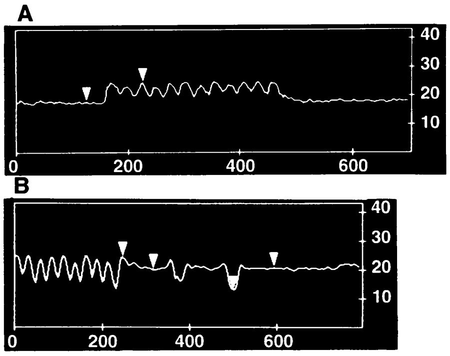

Fig. 3. (**A**) An AFM cross-section profile of unmilled TiO_x-coated S-layers along the line in Fig. 2C. The vertical height difference between the arrowheads is 6.1 nm. (**B**) An AFM cross-section profile of milled TiO_x-coated S-layers along the line in Fig. 2D. The vertical distance between the leftmost set of arrowheads is 4 nm, and the vertical distance between the rightmost set of arrowheads is 8 nm. The erosion of deep holes in the carbon is evident, as are the annular rings of material at the hole edges.

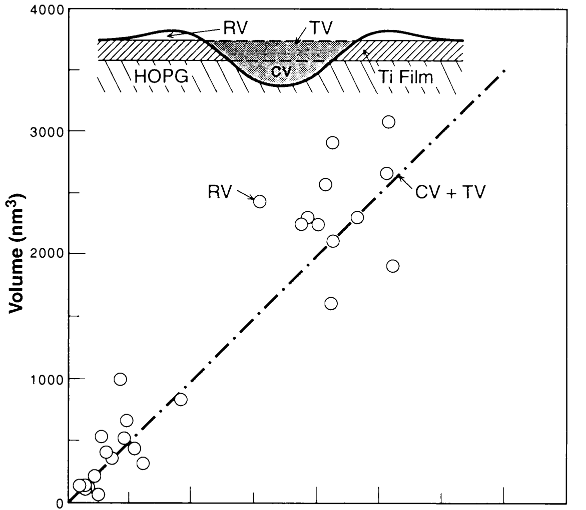

Fig. 4. Annular ring volume, RV (○), and total removed volume, CV + TV (–·–·–), for holes of various sizes. The total removed volume, CV + TV, and annular ring volume, RV, are nearly the same for most holes. Inset: Scale diagram of a 7.5-nm-deep hole showing the annular ring and Ti film.

from the AFM raw data files of off–S-layer holes. In Fig. 4, RV, the annular ring volume (excess volume above the milled TiO_x surface plane) is plotted against CV + TV, the total volume removed (volume missing below the TiO_x surface plane) for a number of different hole sizes. The values for RV lie close to the CV + TV line, indicating that the excess volume of material deposited around the hole circumference is close to the total excess volume of material (both TiO_x and graphite) removed from the hole itself. The convolution of the finite tip radius on the AFM with a small hole profile could cause the measured hole depths to be anomolously low (6). Thus, for smaller holes, RV would be larger than CV + TV, an effect which is in fact not seen in Fig. 4.

It appears that the process of hole formation in the TiO_x film and underlying substrate occurs by heterogeneous nucleation and growth, wherein holes in the TiO_x film open under FAB milling only at nucleation sites (perhaps at nonplanar, thin areas in the TiO_x film). These holes are then further etched into the underlying substrate. On–S-layer, this process is controlled, because the S-layer produces in the TiO_x a periodic array of nucleation sites. The hole formation process is likely to involve both sputtering (removal of material) and redistribution of material induced by ion bombardment. The after-milling TEM image shows that the remaining TiO_x film is continuous. In contrast, at hole sites we observed an erosion of TiO$_x$ at the center of the hole in excess of that observed with the planar TiO$_x$. In addition, the erosion of the carbon is higher than that expected, based on a planar sputtering yield of carbon by 2-keV Ar ions of one ejected atom per ion (*7*). Evolving holes are characterized by spatial variation of the surface composition, surface curvature, and slope, all of which are known to alter sputtering characteristics (*8, 9*). The ring is formed by either reduced erosion near the hole edge or by transport of material from the hole or surrounding area.

REFERENCES AND NOTES

1. K. Douglas, N. A. Clark, K. J. Rothschild, *Appl. Phys. Lett.* **48**, 676 (1986).
2. H. Michel and d.-Ch. Neugebauer, in *Electron Microscopy at Molecular Dimensions*, W. Baumeister and W. Vogell, Eds. (Springer, Heidelberg, 1980), pp. 27–35.
3. R. Prüschenk and W. Baumeister, *Eur. J. Cell Biol.* **45**, 185 (1987).
4. K. A. Taylor, J. F. Deatherage, L. A. Amos, *Nature* **299**, 840 (1982).
5. E. A. Eklund, R. Bruinsma, J. Rudnick, R. S. Williams, *Phys. Rev. Lett.* **67**, 1759 (1991).
6. M. Stedman, *J. Microsc.* **152**, 611 (1988).
7. H. H. Anderson and H. L. Bay, in *Sputtering by Particle Bombardment*, R. Behrisch, Ed. (Springer-Verlag, New York, 1981), chap. 4.
8. H. Oechsner, *Appl. Phys.* **8**, 185 (1975).
9. R. M. Bradley and J. M. E. Harper, *J. Vac. Sci. Technol.* **A6**, 2390 (1988).
10. We thank J. Fleming, B. Holland, and R. Weekley for their technical assistance in this work; J. Peterkin and J. Woollam for the ellipsometry work, and the U.S. Department of Energy Office of Basic Energy Sciences for support through grant DE-FG02-89ER14077.

24 March 1992; accepted 17 June 1992

Sea-Surface Temperature from Coral Skeletal Strontium/Calcium Ratios

J. Warren Beck, R. Lawrence Edwards, Emi Ito,
Frederick W. Taylor, Jacques Recy, Francis Rougerie,
Pascale Joannot, Christian Henin

Seasonal records of tropical sea-surface temperature (SST) over the past 10^5 years can be recovered from high-precision measurements of coral strontium/calcium ratios with the use of thermal ionization mass spectrometry. The temperature dependence of these ratios was calibrated with corals collected at SST recording stations and by ^{18}O/^{16}O thermometry. The results suggest that mean monthly SST may be determined with an apparent accuracy of better than 0.5°C. Measurements on a fossil coral indicate that 10,200 years ago mean annual SSTs near Vanuatu in the southwestern Pacific Ocean were about 5°C colder than today and that seasonal variations in SST were larger. These data suggest that tropical climate zones were compressed toward the equator during deglaciation.

Retrieval of climatic data from the geologic record is important for validating climate models and for understanding the causes of past climate fluctuations. In most climate models, ocean temperature is a crucial parameter because of its linkage with other climate variables such as atmospheric moisture content and temperature, the extent of cloud cover and atmospheric albedo, or the patterns of oceanic and atmospheric circulation. Earlier efforts to recover past ocean temperatures from the geologic record have generally yielded inconsistent results or have proven to be difficult to apply. For example, attempts to recover ocean temperature from the O isotopic composition of biogenic marine carbonate sediments (*1, 2*) have been hampered because we do not know the history of fluctuations in the ocean water ^{18}O/^{16}O ratio, which varies as a function of the volume of the planetary ice caps, or, in the case of sea-surface water, can be modified by rainfall or evaporation effects. Efforts have also been made to reconstruct past ocean temperatures from the records of foraminiferal shell assemblages preserved in deep-sea sediments (*3*) based on knowledge of the temperature controls on modern foraminiferal assemblages (*4*). Such studies suggest that tropical SSTs were 0° to 2°C less than at present during the last glacial maximum (LGM) $\sim$18,000 years ago (*3*). These findings, however, are at variance with estimates of SST based on the elevation of past mountain snow lines, which indicate that tropical SSTs were 3° to 6.5°C lower than at present during the LGM (*5–7*).

One promising method of recovering past SST records involves measuring the Sr/Ca ratios in corals (*8–10*). Scleractinian corals secrete skeletons composed of aragonite (CaCO$_3$), which incorporates both Sr and Ca into its structure. The ratio of incorporation of Sr to Ca is controlled by two factors: the Sr/Ca activity ratio of the ocean water, and the Sr/Ca distribution coefficient between aragonite and seawater (*11, 12*). This latter factor depends on the temperature of the seawater in which the coral grew but is only a weak function of the chemical composition of the seawater. Because of the long residence times of Sr and Ca in the oceans, it is probable that the seawater Sr/Ca ratio has remained essentially constant over time scales of about 10^5 years. Thus, the Sr/Ca ratio of corals is a potential monitor of ocean temperature on these time scales. Earlier work confirmed that coral Sr/Ca ratios reflect SST to a precision of approximately ± 3°C (2σ) (Fig. 1) (*8–10, 13*). However, this precision is about the same as the typical seasonal SST range observed in the tropics where scleractinian corals are found. Longer term variations in global average SST, such as the difference between mean SST for modern times and that at the LGM, may be even smaller than this, perhaps less than 2°C (*3*). Thus, this resolution is inadequate for evaluating seasonal or long-term ocean temperature variability.

In this paper we test the hypothesis that significantly better estimates of SST may be obtained from coral Sr/Ca ratios by improving the measurement precision of this elemental ratio. We first show that considerable improvement in the precision of Sr/Ca measurements can be obtained through use of thermal ionization mass spectrometry (TIMS). Next we assess whether improved analytical precision of this ratio translates into improved accuracy in SST. To do this, we correlated coral Sr/Ca ratios with ocean temperature by measuring ^{18}O/^{16}O ratios on the same coral samples, using the knowledge that coral ^{18}O/^{16}O ratios are a proxy for ocean temperature. Because our corals were collected from ocean island sites adjacent to SST recording stations, the accuracy of the Sr/Ca temperatures was independently assessed by comparison with actual SST measurements. Finally, we discuss the application of this method to recovery of SST from corals that grew during the last deglaciation.

Improved precision in the measurement of coral Sr/Ca ratios was made possible through use of isotope dilution with a triple ^{42}Ca-^{44}Ca-^{84}Sr spike in combination with TIMS (*14*). Both Ca and Sr were loaded

---

J. W. Beck, R. L. Edwards, E. Ito, Minnesota Isotope Laboratory, Department of Geology and Geophysics, University of Minnesota, Minneapolis, MN 55455.
F. W. Taylor, Institute for Geophysics, University of Texas at Austin, Austin, TX 78759.
J. Recy, Antenne ORSTOM (Office de la Recherche Scientifique et Technique d'Outre-Mer), Laboratoire de Geodynamique Observatoire Oceanographique, B.P. 48, 06230 VilleFranche sur Mer, France.
F. Rougerie, ORSTOM de Tahiti, B.P. 529, Papeete, Tahiti, French Polynesia.
P. Joannot, Aquarium de Noumea, B.P. 395, Noumea, New Caledonia.
C. Henin, ORSTOM de New Caledonia, B.P. A-5, Noumea, New Caledonia.